Geomorphology 268 (2016) 246–252

Contents lists available at ScienceDirect

Geomorphology

journal homepage: www.elsevier.com/locate/geomorph

Mechanical conditions and modes of paraglacial deep-seated gravitational spreading in Valles Marineris, Mars

Magdalena Makowska [a,*], Daniel Mège [b,c,d], Frédéric Gueydan [e], Jean Chéry [e]

[a] Institute of Geological Sciences, Polish Academy of Sciences, Research Centre in Wrocław, Poland
[b] Space Research Centre, Polish Academy of Sciences, Warsaw, Poland
[c] Laboratoire de planétologie et géodynamique, Université de Nantes, UMR-CNRS 6112, France
[d] Observatoire des sciences de l'Univers Nantes Atlantique, UMS-CNRS 3281, Nantes, France
[e] Géosciences Montpellier, UMR-CNRS 5243, Université de Montpellier 2, France

ARTICLE INFO

Article history:
Received 15 September 2015
Received in revised form 6 June 2016
Accepted 9 June 2016
Available online 11 June 2016

Keywords:
Deep-seated gravitational spreading
Landslide
FEM
Valles Marineris

ABSTRACT

Deep-seated gravitational spreading (DSGS) affects the slopes of formerly glaciated mountain ridges. On Mars, DSGS has played a key role in shaping the landforms of the giant Valles Marineris troughs. Though less spectacular, DSGS is common in terrestrial orogens, where understanding its mechanics is critical in the light of the ongoing climate change because it is a potential source of catastrophic landslides in deglaciated valleys. We conducted parametric numerical studies in order to identify important factors responsible for DSGS initiation. DSGS models are computed using an elastoviscoplastic finite element code. Using ADELI's software, we reproduce topographic ridge spreading under the effect of valley unloading. Two types of spreading topographic ridges are investigated, homogeneous or with horizontal rheological layering. We find that gravitational instabilities are enhanced by high slopes, which increase gravitational stress, and low friction and cohesion, which decrease yield stress. In the unlayered ridge, instability is triggered by glacial unloading with plastic strain concentration inside the ridge and at the base of the high slopes. Vertical fractures develop in the upper part of the slope, potentially leading to fault scarps. Ridge homogeneity promotes a deformation mode controlled by uphill-facing normal faulting and basal bulging. In the second case, the ridge encompasses horizontal geological discontinuities that induce rock mass anisotropy. Discontinuity located at the base of the slope accumulates plastic strain, leading to the formation of a sliding plane evolving into a landslide. The presence of a weak layer at ridge base therefore promotes another slope deformation mode ending up with catastrophic failure. Mechanical conditions and slope height being equal, these conclusions can probably be extrapolated to Earth. Compared with Mars, DSGS on Earth is inhibited because terrestrial topographic gradients are lower than in Valles Marineris, an effect counterbalanced by increased gravitational stress, where the intensity of deformation is enhanced because of the Earth gravity potential.

1. Introduction

Deep-seated gravitational spreading (DSGS) of slopes affects mountain ridges usually in postglacial conditions (Ballantyne, 2002; Mège and Bourgeois, 2011). Due to ongoing climate change, glacial retreat in many mountains is anticipated to affect slope instability, enhancing DSGS and potentially huge landslides (Hewitt, 2008). The Valles Marineris troughs on Mars provide excellent examples of such relationships among glaciers, DSGS, and huge landslides (Lucas et al., 2001; Mège and Bourgeois, 2011; Gourronc et al., 2014). The DSGS history in Valles Marineris on Mars is rooted in a specific tectonic context that starts with events presenting similarities with rifting in large igneous provinces on Earth. Emplacement of a sequence of thin (typically 50–100 m) layers of volcanic rocks of contrasting strength (McEwen et al., 1999; Beyer and McEwen, 2005), such as basalts and ash or tuff, occurred in response to plume impingement on the base of the lithosphere of the Tharsis dome with a diameter of ca. 5000 km (Mège and Masson, 1996; Mège, 2001). The crust was then stretched, shaping the primary landforms of Valles Marineris (Fig. 1). Evidence for graben development is observed in the southern chasmata (troughs) including Ius, Melas-Candor, Ophir and Coprates: 1) segmented rhombohedral geometry of the floor of some chasmata (Peulvast et al., 2001); 2) the presence of narrow grabens subparallel to the chasma walls on the surrounding plateaus, the fault population distribution of which follows a scaling law that also matches the Valles Marineris dimensions (Schultz, 1997); 3) the chasma floor cratering record, which testifies to plateau subsidence (Blasius et al., 1977; Schultz,

* Corresponding author.
E-mail address: magda.m.makowska@gmail.com (M. Makowska).

http://dx.doi.org/10.1016/j.geomorph.2016.06.011
0169-555X/

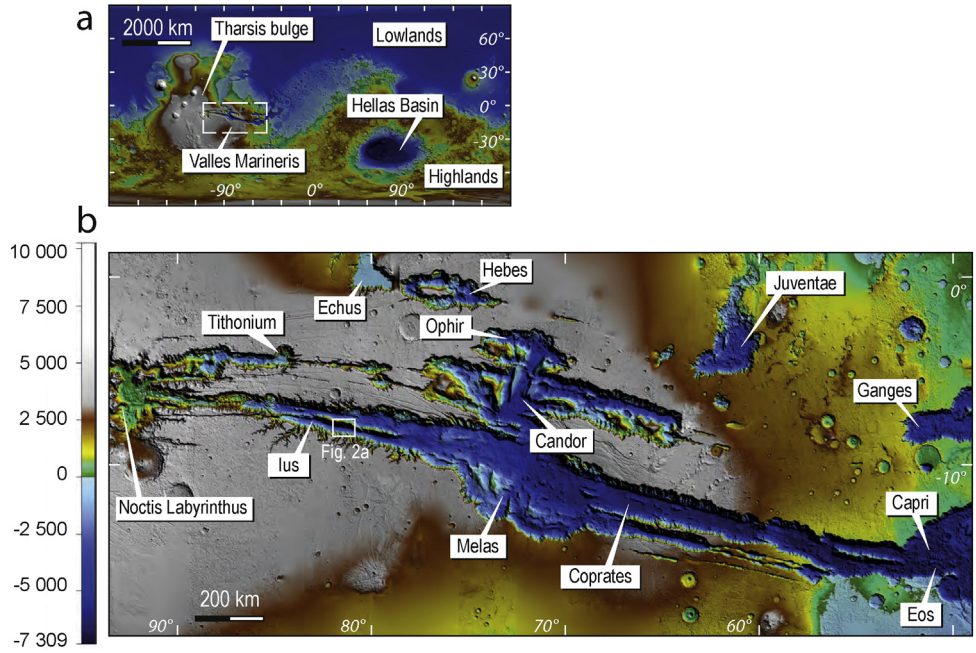

Fig. 1. General setting of Valles Marineris and its troughs (chasmata) on Mars. (a) Location of Valles Marineris. MOLA digital elevation model (NASA/MGS/MOLA), topography varying between −8 km (dark) and 12 km (white). (b) Main chasmata in Valles Marineris. HRSC digital elevation model (ESA/Mars Express/HRSC/DLR/FU Berlin). North is up.

1991); and 4) the presence of triangular faceted spurs (e.g., Hamblin, 1976) on the spur and gully-shaped walls of the chasmata (Peulvast et al., 2001). These indicate that this subsidence was primarily achieved through normal faulting. The Echus, Hebes, and Juventae chasmata do not display such features, suggesting that they have a partly different origin (Schultz, 1998; Jackson et al., 2011). Most observed chasma border fault scarps were removed by further glacial erosion. The fault scarps, located within the inter- and intra-chasma horsts mostly uphill-facing and frequently producing ridge-top grabens, have been interpreted as a result of postglacial deep-seated gravitational spreading (Fig. 2a; Mège and Bourgeois, 2011; Gourronc et al., 2014).

On Earth, from a geomorphological point of view, DSGS refers to movements on high energy hillslopes. These movements affect the whole slope, usually with low displacement rate (Agliardi et al., 2001; Ambrosi and Crosta, 2006). Extension of the upper part of the slope, in the form of tension fractures and uphill-facing normal fault scarps (Jahn, 1964), is balanced by oversteepening of the lower part of the slope (Agliardi et al., 2001; Gutiérrez-Santolalla et al., 2005), sometimes overthrusting the valley (Fig. 2) (Nemcok, 1972).

Nemcok (1972) linked DSGS with post-glacial unloading, which generates fractures parallel to the mountain crest. Forcella and Orombelli (1984) proposed that DSGS faults are a by-product of neotectonic activity. Today, the most commonly accepted interpretation is ridge spreading induced by the release of body forces.

From field observations on the regional context and timing of DSGS, deglaciation appears to play a critical role in DSGS. The loss of lateral ridge buttressing by valley glacier erosion (Agliardi et al., 2001; Cossart et al., 2008; Hippolyte et al., 2009) changes the balance of forces within the ridge, eventually resulting in slope failure. Although most authors have stressed the importance of deglaciation in DSGS; its precise role remains an open question. The major objectives of this study are therefore to constrain i) the role of deglaciation in changing the slope stability, ii) the effect of slope inclination and iii) the influence of weak geological discontinuities on DSGS processes. Besides the

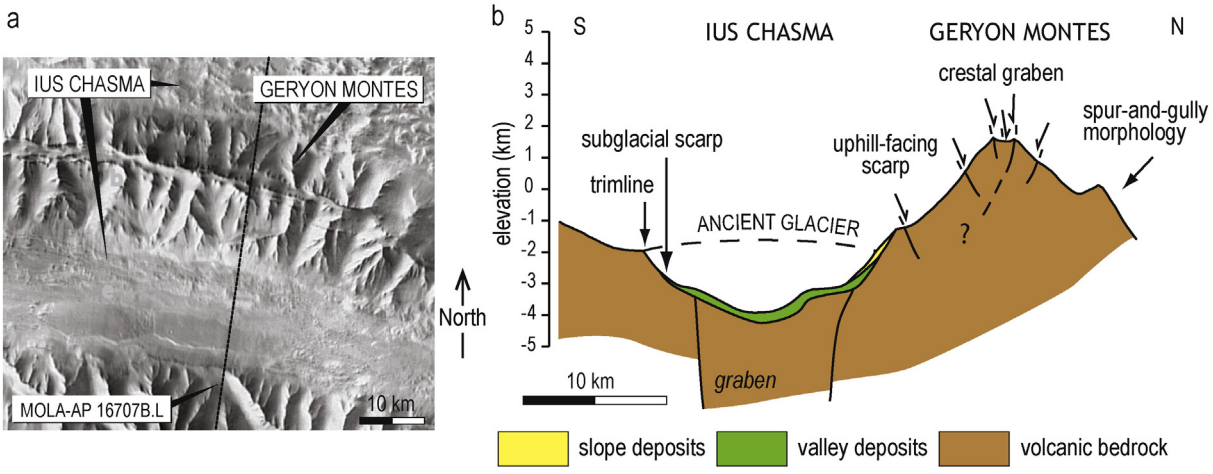

Fig. 2. Deep-seated gravitational spreading on Mars: example at Geryon Montes in Ius Chasma. (a) DSGS affecting the Geryon Montes horst in Valles Marineris with location of MOLA profile MOLA-AP 16707B.L. (b), Geologic interpretation of the MOLA profile
(modified from Mège and Bourgeois, 2011).

interest for the evolution of the Martian slopes and their conditions of development, this understanding has implications for terrestrial DSGS in the light of mountain climate warming (Gruber and Haeberli, 2007) and potential damage that may be caused to hydroelectric power stations, roads, buildings, dams, underground caverns and tunnels (Ambrosi and Crosta, 2006), during the preparatory stage of large-scale, catastrophic landslides (e.g., Hewitt, 2008; Mège and Bourgeois, 2011).

Quantitative understanding of the effects of deglaciation on DSGS development was provided by Agliardi et al. (2001). Their modelling was based on an explicit finite difference method. The role of glacier removal was taken into account by progressive removal of ice sheets to reach post-Würmian conditions. Failure occurs after deglaciation, and produces mass wasting of the upper part of the slope and a bulged morphology at the base. Controlling factors were found to be valley deglaciation and activation of pre-existing fractures. Kinakin and Stead (2005) used the finite difference code FLAC (HCItasca, 2002) to analyse stress distribution in topographic ridges and examine implications for British Columbia and Colorado. These authors pointed out the importance of body forces in formerly glaciated high mountains on slope deformation and the importance of using a rock mass rheology. Finite element modelling (FEM) by Hürlimann et al. (2006) investigated the effect of pre-existing vertical discontinuities on a ridge slope and a weak internal part of the ridge on slope deformation. Bachmann et al. (2009) investigated fracturing during DSGS using the 2-D finite element code ADELI (Hassani, 1994). To trigger slope instability, gravity acceleration was progressively increased until deformation occurred. They showed that the important factors that control fracturing are a reduced rock mass strength and an increased slope height by valley incision.

The present study develops a mechanical approach of DSGS that also makes use of ADELI's finite element code. It provides a systematic parametric study of the mechanical condition for DSGS initiation. The effects of deglaciation on DSGS triggering and evolution with time are investigated along with other parameters, including gravity and geological discontinuities. Both layered and unlayered systems are considered. The effect of slope inclination, angle of internal friction and cohesion on slope stability is quantitatively analysed.

2. Modelling

2.1. Martian study site

DSGS is widespread in Valles Marineris, Mars. Geryon Montes, a horst in Ius Chasma and surrounded by two grabens, is selected for a case study because it represents many DSGS sites in Valles Marineris. It displays a crestal graben in the top of the slope and uphill-facing scarps in the middle (Fig. 2). Spur-and-gully morphology affects the wallslope, below which glacial trimlines are observed, and the lowermost part of the slope is locally folded (Fig. 2). As with most areas in Valles Marineris, the bedrock is composed of a layered volcanic succession observed from the top of the plateau to the debris slope. DSGS triggering is examined in two series of models, corresponding to two geological scenarios pertaining to DSGS occurrences in Valles Marineris (Mège and Bourgeois, 2011). In the first scenario, the topographic ridge is made of homogeneous rocks (unlayered system) that were initially in gravitational equilibrium. The surrounding valleys were initially glaciated, accounting for conditions that may have prevailed in Valles Marineris during much of the Hesperian and Amazonian epochs. Slope destabilization is analysed after valley glacier retreat. Wallrock horizontal layering is taken into account in the second scenario (layered system). The ridge is also in gravitational equilibrium. In the second scenario, thin layers are introduced at three different topographic levels in the ridge, with a weaker rheology than the rest of the ridge. The top layers can be used to study the influence of geological strength contrasts, whereas in the lower portion of the slope, layering may also account for cracks developed by ridge pressurization/depressurization caused by valley glacier buttressing and removal (Cossart et al., 2008).

In the unlayered system, the instability triggering mechanism is erosional activity of the valley glacier combined with ridge rock mass cracking. These factors may cause the effective friction angle and rock mass strength to decrease, resulting in slope stability loss. In the layered system, horizontal geological discontinuities induce oriented rock mass anisotropy. However, in order to characterize the effect of layering and for the sake of simplicity, only three layers are distributed over the whole slope height.

2.2. Model set-up

The models have a symmetric, triangular shape. Boundary conditions are imposed on vertical and lower horizontal borders of the model. Upper horizontal borders are free (Fig 3a). Two types of pressure condition are introduced into the model; lithostatic and glacial pressures. Glacier load affects the horizontal border of the model up to a height of 1 km. Glacier pressure is reduced to 0 in the final time step (Fig. 3b). Decreasing glacier pressure in the models corresponds to the deglaciation stage. The experiments run under Martian gravity, 3.7 m s^{-2}, and are elastically equilibrated at the beginning using a pre-stress model. The models have a slope height of 5 km, corresponding to the average depth of the Valles Marineris chasmata. In order to avoid the effect of boundary conditions, the crust thickness below the ridge is set to 15 km. For layered systems, the density, effective friction angle and cohesion of the introduced thin layers are reduced by 20% compared with the ridge in order to generate a rheological contrast. This difference accounts for the lower strength of pyroclastic rocks compared with the strength of basaltic lava flows. Slope inclination, angle of internal friction, and cohesion are variable parameters. Studying deformation on Mars requires some assumptions because direct measurements of mechanical parameters for Martian rocks are not available. Rock density ρ, Young's modulus E, and the Poisson ratio ν are taken from experimental data for terrestrial basalts. The values of E and ν used in this study are respectively 1 GPa and 0.25 corresponding to estimation by Schultz (1995). The density is at the lower end of the density range for basalts (2.8 g cm^{-3}). The angle of internal friction φ, cohesion c, angle of dilatancy ψ, and inclination of the slope α are model variables.

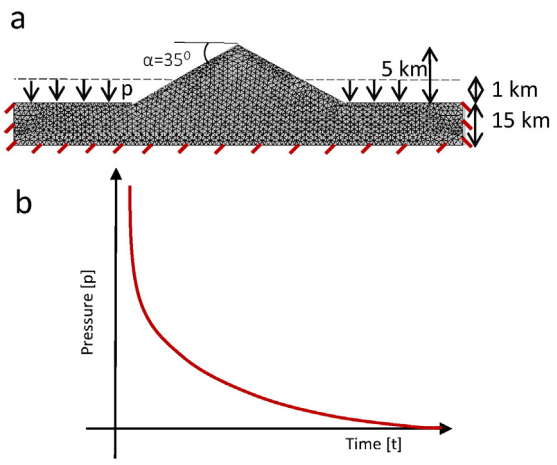

Fig. 3. Model set-up. (a) Mesh geometry. Diagonal lines indicate fixed boundary condition. Dashed lines indicate maximum height of imposed pressure condition on the wallslopes corresponding to the maximum level of the removed glacier. (b), Glacial pressure dependency of time.

2.3. Numerical approach

Two-dimensional simulations were performed using the ADELI code (Hassani, 1994). The method is based on subdivision of a solid body into an equivalent system of triangular elements interconnected at nodes. The number of building elements is approximately 50,000 (Fig. 3). Strain and stress calculations are done for each element, and are subsequently combined to obtain the solution for the whole body.

ADELI has been used to solve 2D and 3D geological problems involving the thermo-mechanical behaviour of the crust and the lithosphere at geologic time scale (e.g., Hassani et al., 1997). Constitutive equations include various rheologic properties: elastic, elastoplastic, viscoelastic and body forces corresponding to a constant gravity field. The boundary conditions as well as initial stress and temperature can be adjusted.

2.4. Model rheology

We used an elasto-plastic constitutive law associated with a Drucker–Prager rheology. The Drucker–Prager yield criterion is given as:

$$\sqrt{J_2} = A + BI_1 \quad (1)$$

where I_1 is the first invariant of Cauchy stress, J_2 is the second invariant of the deviatory part of the Cauchy stress, and A and B are experimentally determined constants.

This criterion is expressed as (Drucker and Prager, 1952):

$$\sigma_e = a + b\sigma_m \quad (2)$$

where σ_e is the equivalent stress, σ_m is hydrostatic stress, and a and b are material constants.

3. Results

Nearly 120 scenarios were run, with slope inclination α between 20° and 35°. This inclination is representative of internal bedrock ridge slopes in Valles Marineris (Crosta et al., 2014). The angle of dilatancy ψ, which controls volumetric plastic strain during shearing, is between $1/4\varphi$ and $1/3\varphi$. Instability initiation is studied as a function of three variables: slope inclination, angle of internal friction, and cohesion. Figs. 4 and 5 show the final time steps, after glacial unloading.

3.1. Unlayered ridge

The results of models having relatively steep slope ($\alpha = 35°$, Fig. 4c–h) show that strain concentrates in two regions in the ridge, the core and base. These patterns of deformation are due to stress release and loss of support after glacier retreat. Ridge core strain occurs across the whole ridge thickness and ends upwards with a diffuse zone of deformation on both sides of the ridge. Deformation of the ridge base corresponds to ridge bulging or even overthrusting (Beget, 1985; Savage and Varnes, 1987; Varnes et al., 1989; Chigira, 1992; Retiner et al., 1993). At high φ (Fig. 4e, f), the top of the deformed core is deeper, producing ridge top splitting, which is the most spectacular criterion for DGS identification. At $\varphi = 40°$, the diffuse zone at the top of the ridge transforms to steeply dipping cracks. With increasing cohesion (Fig. 4i), up to 10.0 MPa, deformation does not exceed elasticity.

Changing the slope inclination (Fig. 4a) affects the gravitational potential of the ridge. For gentle slopes, the strain accumulated in the ridge core. Strain dependency on the friction angle (Fig. 4d–f) is more significant than slope dependency (Fig. 4a–c). The increase of internal friction angle lowers the concentration of plastic strain in the core and base of the ridge. At $\varphi = 40°$, (Fig. 4f) nearly vertical fractures located at the top of the hill are the only significant ridge deformation. φ is a key factor for controlling fault angle. Because the hydrostatic load of the glacier is lower than the rock weight, the normal stress σ_1 is vertical. Considering that the dip angle of a fault in unfractured rock is $\pi/4 + \varphi/2$, for $\varphi = 15°$ the dip of the fault is equal to 52.5°. This value is larger than the slope inclination, implying that the slope is stable. For φ lower than 15°, connection of two strain zones (core and base) may lead to the formation of a low-angle fault with very small displacement. Consistently, increasing φ increases the dip angle of the fault and promotes gravitational stability.

The concentration of plastic strain is also significantly dependent upon cohesion, which controls the value of the shear stress required for fracturing (Fig. 4c). For $c = 1.5$ MPa, plastic strain concentrates in the core zone and at the base of the ridge. The core zone deformation propagates upward to the top of the ridge. With increasing c, the size of the deformed core zone significantly decreases (6 MPa) then disappears (10 MPa). When c is equal to 6.0 or 10.0 MPa, yield strength is larger than the deviatoric stress induced by gravity forces and there is no localized fracturing but a distributed elastic deformation. This result is consistent with the observation that high cohesion (10 MPa), achieved in intact rock but not in natural rock masses (e.g. Schultz,

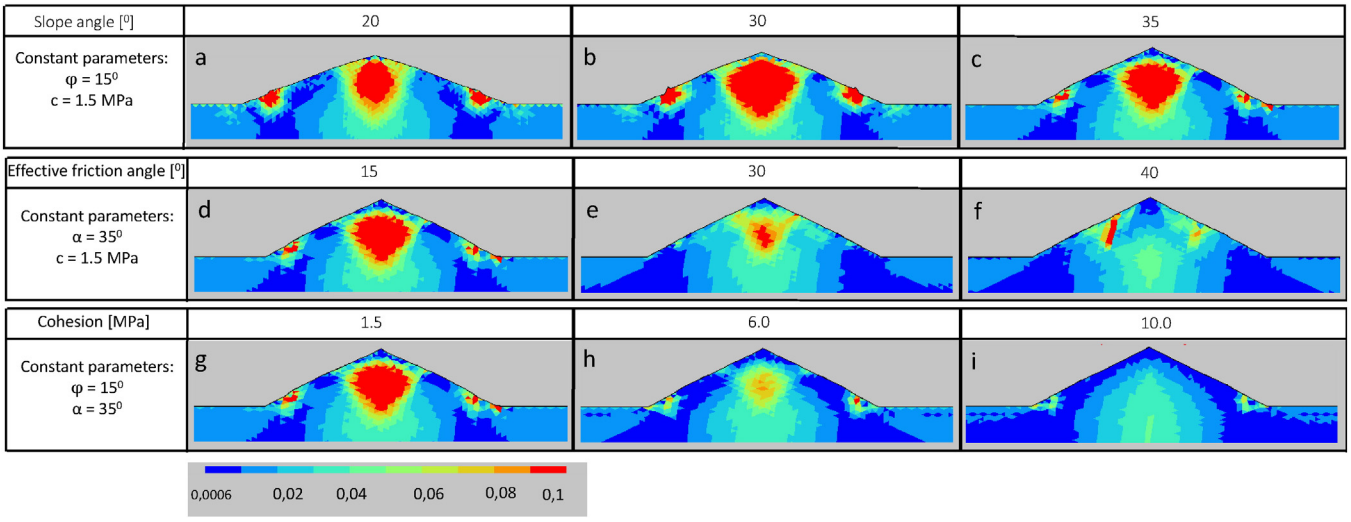

Fig. 4. Final time steps of unlayered ridge system modelling showing gravitational instability developed under various conditions of slope inclinations (a to c), effective friction angles (d to f), and cohesions (g to i). Plastic strain varies from 0.0001 (blue) to 0.1 (red). Only the upper 4 km of the crust are displayed. (For interpretation of the references to colour in this figure legend, the reader is referred to the web version of this article.)

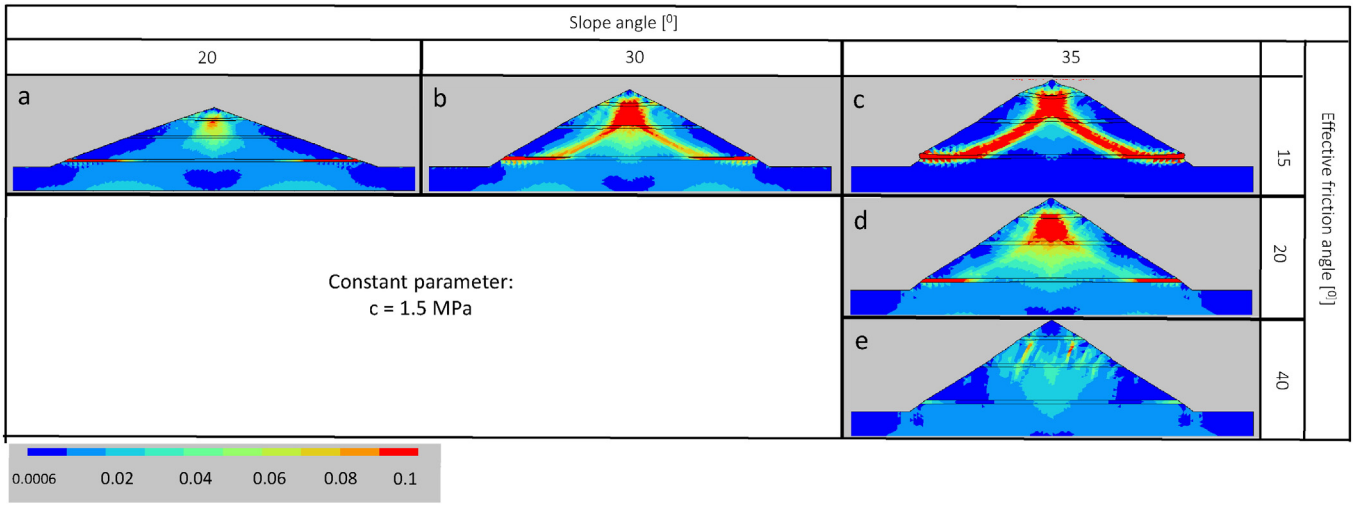

Fig. 5. Final time steps of layered ridge system modelling showing the role of slope inclination (a to c) and effective friction angle (c to e) on ridge gravitational instability for constant cohesion. Plastic strain varies from 0.0001 (blue) to 0.1 (red). Only the upper 4 km of the crust are displayed. (For interpretation of the references to colour in this figure legend, the reader is referred to the web version of this article.)

1996), is able to prevent significant deformation to occur. Large mass wasting processes such as landsliding are not predicted, whereas uphill-facing scarp is expected.

3.2. Layered ridge

The model with slope $\alpha = 35°$, $c = 1.5$ MPa and $\varphi = 15°$ (Fig. 5c) displays two failure surfaces developing along the whole ridge height, connecting a strained zone at the top of the ridge to strain in the lower weak layer. The orientation of these planes compared with the orientation of the principal stress trajectories indicates that they are normal faults, and landsliding is expected. The weak layer at the base of the ridge is an area of intense strain focus. The core and the basal plastic strain concentration zones merge into a large deformation zone. Horizontal sliding along the pre-existing layer and fracturing higher within the ridge result in two well-defined failure surfaces. Increasing φ gradually limits or inhibits the development of these planes (Fig. 5d, e). At $\varphi = 40°$, they are replaced by vertical cracks at the top of the model (similar to those observed in the unlayered set-up). At moderate $\varphi = 20°$ (Fig. 5d), most plastic strain accumulates in the ridge core. Plastic strain concentrates along the weak base layer of the model.

With $\alpha = 20°$ (Fig. 5a), the low gravitational potential is not sufficient for failure planes to develop. Comparison with the ridge strain distribution of a homogeneous ridge with the same mechanical parameters (Fig. 4a) shows that the strained core zone is much smaller with layering than without it. Basal deformation concentrates in the weak layer at the base of the slope. Development of mountain-scale

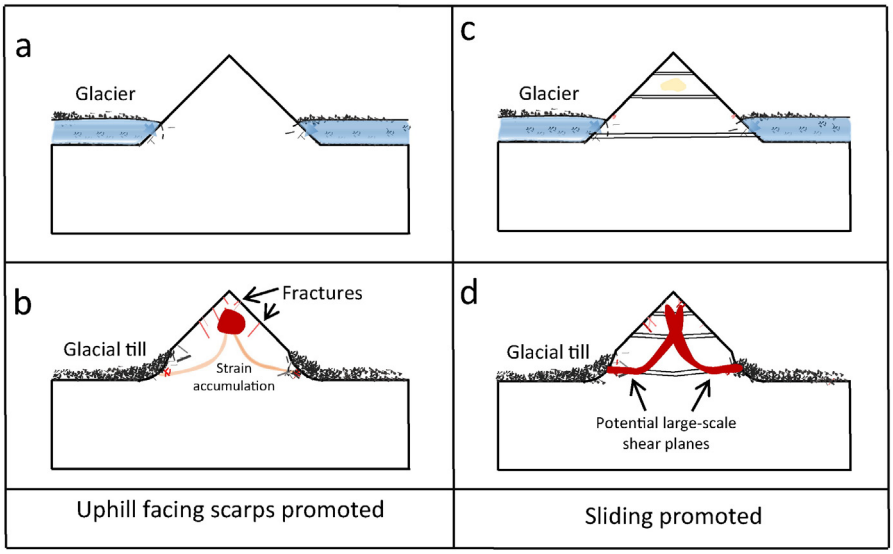

Fig. 6. Two end-member scenarios of DSGS development, resulting in final profiles displaying ridge-top splitting and uphill-facing scarp development (a and b) or landsliding (c and d). In the first scenario, the ridge is unlayered and initially in gravitational equilibrium. The floor of the surrounding valleys is initially covered by glaciers (a). Glacial water infiltrates the microcracks and fractures at the bottom of the ridge. During glacier retreat, the fractures grow, and new discontinuities initiate and develop, especially at the top of the ridge (b). A vertical failure surface develops at the upper part of the ridge as a result of strain regime change. Glacial erosion produces trimline-capped subglacial scarps and till accumulation in the valley. Conditions for sliding are not optimal. In the second scenario, the ridge is layered and in gravitational equilibrium. Cracks present at the base of the slope are exposed to erosion by glacial water (c) resulting in weakening of the lower layer. Limited strain accumulates in this weak layer and above it, at the core of the ridge. (d) More strain accumulates further in the weak layers and within the ridge. After glacier retreat, slope profile has considerably changed and is no longer gravitationally stable. Although uphill-facing scarps may have developed, further sliding is promoted. Black accumulation are glacial till deposits. Colours represent accumulation of plastic strain: light red – small accumulation of plastic strain, red – high accumulation of plastic strain. (For interpretation of the references to colour in this figure legend, the reader is referred to the web version of this article.)

normal fault planes occurs starting from $\alpha = 30°$ (Fig. 5b). Maximum strain along the failure surfaces occurs for the steepest slopes (Fig. 5c–e).

4. Discussion

Most experiments produce significant ridge deformation, a feature consistent with the observation in Valles Marineris, where steep slopes are systematically affected by DSGS (Mège and Bourgeois, 2011).

In the unlayered models (Fig. 6a, b), development of gravitational instabilities is limited to the lowermost part of the ridge, and in the upper slope, to fault scarps that do not evolve to sliding planes. Steep faults end at depth without connecting to a low-angle plane and generate a continuous shear plane. This situation corresponds to Fig. 2b, where landsliding is not observed. There are three possibilities: i) landsliding may occur in the future; ii) in this area of Valles Marineris, bedrock layering does not provide enough strength contrast for sliding planes to develop; and iii) the layered bedrock may behave mechanically as homogeneous at ridge scale. The basal slope deformation observed in all the unlayered experiments has been reported in Valles Marineris (Mège and Bourgeois, 2011), but in most cases the systematic occurrences of huge debris slopes may hide the topography of the wallrock behind.

Huge landslides, as predicted in the layered models (Fig. 6c, d), are also observed in Valles Marineris. Observational evidence (Mège and Bourgeois, 2011) as well as modelling of debris apron geometry (Lucas et al., 2001) indicate that it represents a further evolution of DSGS. In most cases, the two failure planes are not expected to evolve toward sliding planes, except in the unlikely case where sliding would be synchronous, because the first landslide would immediately reorganize the stress distribution in the ridge and limit the activation of the second plane.

In order to assess how these results may be extrapolated to the environment of the Earth, two runs were conducted with gravity set at 9.8 m s^{-2}. Fig. 7 shows how these results compare with results obtained under Martian gravity, all the other parameters being the same. On Earth (Fig. 7c, d), plastic strain concentrates in the core and base of the ridge like in the Mars environment (Fig. 7a, b). The distribution of strain is similar, favouring vertical cracks in layered ridge and ridge core deformation in homogenous ridge. However, the accumulated strain is significantly larger on Earth. DSGS is predicted (and observed) to be very frequent on Mars, and it is predicted to be similar on Earth under the same condition. The Earth experiment reported on Fig. 7d is the only one that predicts significant strain in a weak layer that is not the basal layer. All the models were set with a slope height of 5 km, which is representative of slopes in Valles Marineris, but is never attained on Earth at the scale of individual topographic ridges. The rarer occurrences of DSGS in terrestrial mountains compared with the studied Martian mountains are therefore explained by significantly lower slope gradient.

Fig. 7 suggests that in contrary to the intensity of deformation, the *style* of deformation on Mars and Earth is similar for the same values of mechanical parameters. This is illustrated with the well-studied Chabenec ridge in the Slovakian Tatras (Nemcok, 1972; Mahr and Nemcok, 1977), where both uphill-facing fault scarps and intense basal deformation are observed, but no sliding plane are found between these deformed areas. The Chabenec ridge is composed of a diorite and granodiorite rock mass (Nemcok, 1972), and is therefore not layered. Chabenec is in the situation depicted on Fig. 4e, with friction and cohesion being ca. 30° and 1.5 MPa, respectively, if it were located on Mars.

5. Summary

FEM modelling allowed the successful reproduction of DSGS observations on Mars, and constrained the controlling parameters responsible for strain localization. Crucial factors for slope instability in Martian environment are a weak rheology, including low values of plastic yield stress (e.g., φ 15°–20°) and cohesion (1.5 MPa), and high slopes. Glacier retreat from the valleys is a crucial factor for initiation of DSGS provided that it interplays with favourable factors like weak rheology, presence of fissures, cracks, joints, slope height and possibly a regional isostatic adjustment (Ustaszewski et al., 2008).

Two modes of slope deformation have been identified. In homogeneous ridges uphill-facing scarps, ridge-top grabens, and basal bulging are favoured. In contrast, in rheologically layered rock, landsliding is promoted. Development of sliding surfaces is triggered by the connection between a horizontal plane along pre-existing zone, and fracturing in the core of the ridge. This connection is possible only for steep slopes and weak rheology (low φ and low c). It is plausible that in ridges having a basal level weakened by groundwater circulation, the first DSGS mode may initiate and gradually turn to the second mode, forming uphill-facing scarps and ridge-top grabens that may later evolve to large-scale landsliding. The triggering mechanisms are expected to be similar for Martian and terrestrial ridges having similar

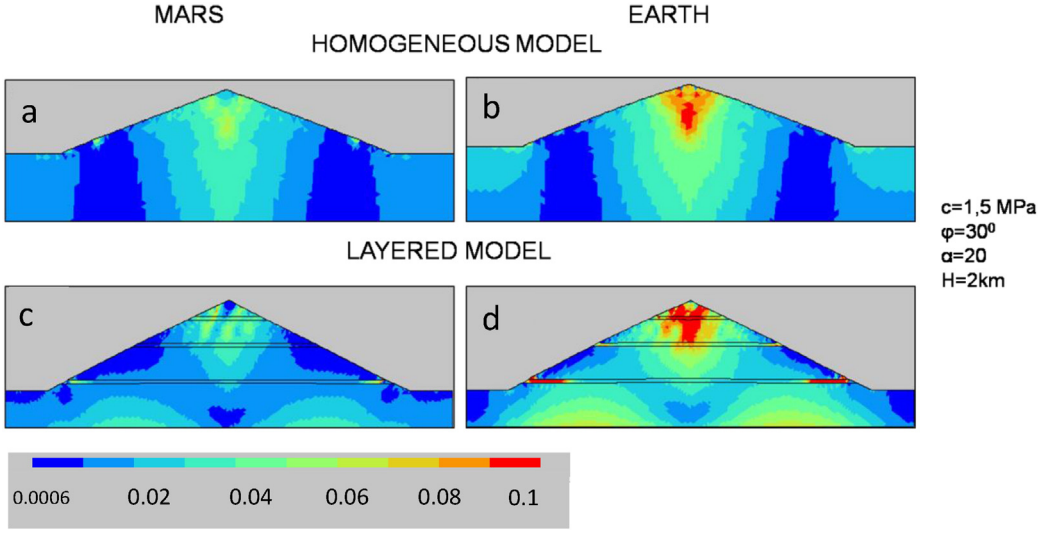

Fig. 7. Final steps of models run in Mars gravity conditions, g = 3.7 m s^{-2} (a and c) and in Earth gravity conditions, g = 9.8 m s^{-2} (b and d). Slope inclination (α), angle of internal friction (φ), cohesion (c), and height (H) are the same in both models. Plastic strain varies from 0.0001 (blue) to 0.1 (red). Only the upper 4 km of the crust are displayed. (For interpretation of the references to colour in this figure legend, the reader is referred to the web version of this article.)

morphology; the lower slopes on Earth tend to inhibit DSGS, while higher gravity tends to enhance it.

Acknowledgments

This work was supported by the TEAM programme of the Foundation for Polish Science (project TEAM/2011-7/9), co-financed by the European Union within the framework of the European Regional Development Fund. Thanks are especially directed to Joanna Gurgurewicz, whose dedication to this project made this work possible. Thanks are extended to the anonymous reviewers, and to Editor Takashi Oguchi for significant editorial improvements. The authors thank Paweł Skiścim for technical help with ADELI.

References

Agliardi, F., Crosta, G., Zanchi, A., 2001. Structural constraints on deep-seated slope deformation kinematics. Eng. Geol. 59, 83–102.
Ambrosi, C., Crosta, G.B., 2006. Large sackung along major tectonic features in the Central Italian Alps. Eng. Geol. 83, 183–200.
Ballantyne, C.K., 2002. Paraglacial geomorphology. Quat. Sci. Rev. 21, 1935–2017.
Bachmann, D., Bouissou, S., Chemenda, A., 2009. Analysis of massif fracturing during deep-seated gravitational slope deformation by physical and numerical modeling. Geomorphology 103, 130–135.
Beget, J.E., 1985. Tephrochronology of antislope scarps on an alpine ridge near Glacier Peak, Washington, U.S.A. Arctic Apline Res. 17, 143–152.
Beyer, R.A., McEwen, A.S., 2005. Layering stratigraphy in eastern Coprates Chasma and northern Capri Chasma. Icarus 179, 1–23.
Blasius, K.R., Cutts, J.A., Guest, J.E., Masursky, H., 1977. Geology of the Valles Marineris: first analysis of imaging from the Viking 1 orbiter primary mission. J. Geophys. Res. 82, 4067–4091.
Chigira, M., 1992. Long-term gravitational deformation of rock by mass rock creep. Eng. Geol. 32, 157–184.
Cossart, E., Braucher, M., Bourlès, D.L., Carcaillet, J., 2008. Slope instability in relation to glacial debuttressing in alpine areas (Upper Durance catchment, southeastern France): evidence from field data and ^{10}Be cosmic ray exposure ages. Geomorphology 95, 3–26.
Crosta, G.B., Utili, S., De Blasio, F.V., Castellanza, R., 2014. Reassessing rock mass properties and slope stability triggering condition in Valles Marineris, Mars. Earth Planet. Sci. Lett. 388, 329–342.
Drucker, D.C., Prager, W., 1952. Soil mechanics and plastic analysis for limit design. Q. Appl. Math. 10, 157–165.
Forcella, F., Orombelli, G., 1984. Holocene slope deformations in Valfurva, Central Alps Italy. Geogr. Fish. Dinam. Q. 7, 41–48.
Gourronc, M., Bourgeois, O., Mège, D., Pochat, S., Bultel, B., Massé, M., Le Deit, L., Le Mouélic, S., Mercier, D., 2014. One million cubic kilometres of fossil ice in Valles Marineris: relicts of a 3.5 Gy old glacial landsystem along the Martian equator. Geomorphology 204, 235–255.
Gruber, S., Haeberli, W., 2007. Permafrost in steep bedrock slopes and its temperature-realted destabilization following climate change. J. Geophys. Res. 112. http://dx.doi.org/10.1029/2006JF000547 (F02S18).
Gutiérrez-Santolalla, F., Gutiérrez-Elorza, M., Marín, C., Maldonado, C., Younger, P.L., 2005. Subsidence hazard avoidance based on geomorphological mapping in the Ebro River valley mantled evaporite karst terrain (NE Spain). Environ. Geol. 48, 370–383.
Hamblin, W.K., 1976. Patterns of displacement along the Wasatch fault. Geology 4, 619–622.
Hassani, R., 1994. Modélisation numérique de la déformation Des systêmes géologiques Thèse de Doctorat Université de Montpellier II, France.
Hassani, R., Jongmans, D., Chéry, J., 1997. Study of plate deformation and stress in subduction processes using two-dimensional numerical models. J. Geophys. Res. 102, 17,951–17,965.
HCltasca, 2002. FLAC 4 Users Guide. Itasa Consulting Group, Minneapolis, MN http://www.hcitasca.com.
Hewitt, K., 2008. Legacies of catastrophic rock slope failures in mountain landscapes. Earth Sci. Rev. 87, 1–38.
Hippolyte, J.-C., Bourlès, R., Carcaillet, J., Léanni, L., Arnold, M., Aumaitre, G., 2009. Cosmogenic ^{10}Be dating of sacking and its faulted rock glacier, in the Alps of Savoy (France). Geomorphology 108, 312–320.
Hürlimann, M., Ledesma, A., Corominas, J., Prat, P.C., 2006. The deep-seated slope defomation at Encampadana, Andorra: representation of morphologic features by numerical modelling. Eng. Geol. 86, 343–357.
Jackson, M.P.A., Adams, J.B., Dooley, T.P., Gillespie, A.R., Montgomery, D.R., 2011. Modeling the collapse of Hebes Chasma, Valles Marineris, Mars. GSA Bull. 123, 1596–1627.
Jahn, A., 1964. Slope morphological features resulting from gravitation. Z. Geomorphol. Suppl.bd 5, 59–72.
Kinakin, D., Stead, D., 2005. Analysis of the distributions of stress in natural ridge forms: implications for the deformation mechanism of rock slopes and the formation of sacking. Geomorphology 65, 85–100.
Lucas, A., Mangeney, A., Mège, D., Bouchut, F., 2001. Influence of the scar geometry on landslide dynamics and deposits: application to Martian landslides. J. Geophys. Res. 116, E10001. http://dx.doi.org/10.1029/2011JE003803.
Mahr, T., Nemcok, A., 1977. Deep seated deformations in the crystalline cores of the Tatry Mts. Int. Assoc. Eng. Geol Bull. 16, 104–106.
McEwen, A.S., Malin, M.C., Carr, M.H., Hartmann, W.K., 1999. Voluminous volcanism on early Mars revealed in Valles Marineris. Nature 397, 584–586.
Mège, D., 2001. Uniformitarian plume tectonics: the post-Archean Earth and Mars. In: Ernst, R.E., Buchan, K.L. (Eds.), Mantle Plumes: Their Identification through Time. Geol. Soc. Am. Spec. Pap. 352, pp. 141–164.
Mège, D., Bourgeois, O., 2011. Equatorial glaciations on Mars revealed by gravitational collapse of Valles Marineris wallslopes. Earth Planet. Sci. Lett. 310, 182–191.
Mège, D., Masson, P., 1996. A plume tectonics model for the Tharsis province, Mars. Planet. Space Sci. 44, 1499–1546.
Nemcok, A., 1972. Gravitational slope deformation in high mountains. Proc. 24th Int. Geol. Congr.,. 13, pp. 132–141.
Peulvast, J.-P., Mège, D., Chiciak, J., Costard, F., Masson, P.L., 2001. Morphology, evolution and tectonics of Valles Marineris wallslopes (Mars). Geomorphology 37, 329–352.
Retiner, J., Lang, M., van Husen, D., 1993. Deformation of high slopes in different rocks after würmian deglaciation in the Gailtal (Austria). Quat. Int. 18, 43–51.
Savage, W.Z., Varnes, D.J., 1987. Mechanics of gravitational spreading of steep-sided ridges ("sackung"). Bull. Int. Assoc. Eng. Geol. 35, 31–36.
Schultz, R.A., 1991. Structural development of Coprates Chasma and western Ophir Planum, Valles Marineris rift, Mars. J. Geophys. Res. 96, 22,777–22,792.
Schultz, R.A., 1995. Limit on strength and deformation properties of jointed basaltic rock masses. Rock Mech. Rock. Eng. 28, 1–15.
Schultz, R.A., 1996. Relative scale and the strength deformability of rock masses. J. Struct. Geol. 18, 1139–1149.
Schultz, R.A., 1997. Displacement–length scaling for terrestrial and Martian faults: implications for Valles Marineris and shallow planetary grabens. J. Geophys. Res. 102, 12,009–12,015.
Schultz, R.A., 1998. Multiple-process origin of Valles Marineris basins and troughs, Mars. Planet. Space Sci. 46, 827–834.
Ustaszewski, M.E., Hampel, A., Pfiffner, O.A., 2008. Composite faults in the Swiss Alps formed by the interplay of tectonics, gravitation and postglacial rebound: an integrated field and modelling study. Swiss J. Geosci. http://dx.doi.org/10.1007/s00015-008-1249-1.
Varnes, D.J., Radbruch-Hall, D.H., Savage, W.Z., 1989. Topographic and structural conditions in areas of gravitational spreading of ridges in the western United States. US Geol. Surv. Prof. Pap. 1496 (28 pp.).